Ceramics International 43 (2017) 15459–15465

Contents lists available at ScienceDirect

Ceramics International

journal homepage: www.elsevier.com/locate/ceramint

Sintering induced the failure behavior of dense vertically crack and lamellar structured TBCs with equivalent thermal insulation performance

Bo Cheng, Ning Yang, Qiang Zhang, Meng zhang, Yu-Ming Zhang, Lin Chen, Guan-Jun Yang*, Cheng-Xin Li, Chang-Jiu Li

State Key Laboratory for Mechanical Behavior of Materials, School of Materials Science and Engineering, Xi'an Jiaotong University, Xi'an, Shaanxi Province 710049, PR China

ARTICLE INFO

Keywords:
Thermal cyclic lifetime
Thermal barrier coatings (TBCs)
Plasma spray
Equivalent thermal insulation
Dense vertically crack (DVC)

ABSTRACT

Both thermal cyclic lifetime and thermal barrier performance are essentially important to the application of thermal barrier coatings (TBCs). In this study, equivalent thermal insulation conception is introduced to the design of TBCs to fairly compare different structured TBCs. Dense vertically crack (DVC) structured TBCs and the lamellar structured TBCs with same top coat thickness of 1000 μm (D1000 and L1000), and lamellar structured TBCs with 570 μm (L570, equivalent thermal insulation performance with D1000) top coat were prepared. Their lifetimes were evaluated under gradient thermal cyclic test. D1000 TBC shows a rather longer lifetime than L1000 TBC because of the alleviation of vertically cracks, but D1000 TBC possesses a much lower thermal barrier performance than L1000 TBC due to the dense structure of D1000 TBC. However, for the TBCs with the same equivalent thermal insulation performance, L570 TBC presents a more than two times longer lifetime than D1000 TBC. TGO thickening and phase transformation were proved not responsible for the failure of L1000 and D1000 TBCs in the present condition. The in-plane elastic modulus and Vickers hardness across top coat thickness were examined, and the results proved that the mechanical evolution of the top coat after high temperature exposure resulting in the competition between driving force and cracking resistance dominates the failure behavior of TBCs. This study is beneficial for the comprehensively understanding of the failure behavior of DVC and lamellar structured TBCs, and thereby shed light to further coating structure optimization and design innovation.

1. Introduction

Thermal barrier coatings (TBCs) are frequently used to provide thermal and corrosion protections for the metallic hot-section components of both aircraft engines and land-based gas turbines to achieve higher turbine inlet temperature and extended durability [1–4]. The TBC system consists of a nickel or cobalt based superalloy; a substrate-composition-similar, MCrAlY(M = Ni, Co, NiCo, CoNi) or NiAl-based bond coat (BC); a ceramic coat on the top of the TBC system to provide thermal protection for the substrate [5,6]. 7–8 wt% yttria-stabilized zirconia (8YSZ) is the state-of-the-art top coat TBC material, primarily due to its low thermal conductivity, high toughness and high coefficient of thermal expansion (CTE) [7–10].

Air plasma spraying is a most important method used for TBC top-coat deposition [8,11]. APS TBCs have the favorable lamellar microstructure (contributes to approximately half more drop as respect to its corresponding bulk material in the through-thickness direction) to provide a good thermal insulation performance [1,12,13]. However, during extended time high temperature exposure, the sintering of ceramic coating inevitable happened, companying the partial disappearance of the lamellar microstructure, leading to significant stiffening of the top coat. This has a great contribution on the driving force for the premature failure of TBCs [14,15].

Vertical micro cracks are deliberately introduced in the ceramic top coat to relieve stresses of TBC system during high temperature exposure which named DVC (dense vertically-cracked) TBCs [16,17]. It has been reported that the DVC structure extended the TBC lifetime compared with the same top coat thickness [18,19]. The prime characteristic of DVC TBCs is the vertically micro cracks in the top coat, which relieve stresses and at the same time, weaken the thermal insulation performance of TBCs. Therefore, DVC TBCs are always been deposited with a thicker top coat to ensure the

* Corresponding author.
E-mail address: ygj@xjtu.edu.cn (G.-J. Yang).

http://dx.doi.org/10.1016/j.ceramint.2017.08.092
Received 28 June 2017; Received in revised form 10 August 2017; Accepted 14 August 2017
Available online 16 August 2017

thermal insulation performance. For DVC TBCs, the unique microstructures can be achieved under conditions involving plasma spraying at high power, high powder flow rates, carefully controlled spray distances, or relatively high substrate temperatures (e.g., > 400 °C) [20,21]. Under the condition mentioned above, the coating may have a density greater than about 88% of theatrical to ensure the homogeneous formation of vertical cracks [16]. This increases the bond strength of top coat and may extend the TBC lifetime at a certain degree.

Lamellar structured TBCs shows an excellent thermal barrier performance when compared with the DVC TBCs [19,21,22], however, the stress during high temperature exposure may not be relieved readily. This may be an inducement for the failure of TBCs. The vertically cracks in the DVC system can effectively absorb the stress [23,24] caused by the sintering effect, and at the same time, the dense microstructure is favorable for the increase of cracking resistance. In most cases, DVC TBCs were compared with the lamellar ones under the condition of some top coat thickness [18,19]. It should be well addressed that the dense structure of DVC TBC significantly reduces the thermal barrier performance. In order to possess the same thermal barrier performance as lamellar structured TBC, DVC TBC has to increase the top coat thickness. However, this, in turn, increases both the preparation cost and the weight of hot section parts, which are definitely not expected.

In this study, DVC structured and lamellar structured TBCs were prepared under the premise of same top coat thickness and thermal insulation performance. The main objective of the present work is to comprehensively understanding the failure behavior of DVC and lamellar structured TBCs.

2. Experimental procedure

2.1. Material and preparation

The dense vertically-cracked plasma-sprayed coatings used in this study were supplied by a commercial coating manufacturer. For the lamellar structured TBCs, a commercial spherical YSZ powder (Sulzer Metco 204NS-G, −125 + 11 μm) were used to deposit the ceramic top coat by an APS system (GP-80, JiuJiang, China). The spray parameters were shown in Table 1. Prior to the deposition of the top-coat, a commercially available NiCoCrAlTaY powder (Amdry 997, −37+9 μm, Sulzer Metco, Westbury, NY) was used as the bond coat. YSZ and NiCoCrAlTaY powder was shown in Fig. 1(a) and (b), the inset shows the hollow cross section of a powder particle. The bond coat was deposited on a nickel-based superalloy (Inconel 738, Φ25.4 mm × 3 mm) substrate. In order to reduce edge effects, the rim of the substrate was rounded. The bond coat was deposited to approximately 150 μm by a low pressure plasma spraying (LPPS) system. Table 2 shows the spraying parameters of LPPS. The thickness of top-coat was approximately 1000 μm and 570 μm. Before the deposition of top-coat, the as-prepared samples with bond-coat were subjected to a preheat-treatment to forming a dense and connective Al_2O_3 TGO. The preheat-treatment process consists of two steps, namely, a pre-diffusion procedure (1080 °C +4 h, $O_2 \leq 0.01$ ppm) following by a pre-oxidation procedure (1080 °C +4 h, $O_2 \approx 10$ ppm).

Table 1
Parameters of air plasma spraying for top coating.

Parameters	YSZ (Lamellar)
Arc current, A	650
Arc voltage, V	60
Primary plasma gas (Ar) flow, L/min	50
Secondary plasma gas (H_2) flow, L/min	7
Spray distance, mm	80

2.2. Characterization

The cross-sectional microstructure of the coating was investigated using a scanning electron microscope (SEM) system (TESCAN MIRA 3 LMH, Czech Republic). Before obtaining the section of samples for a metallographic examination, the samples were infiltrated with epoxy adhesive in vacuum to protect the coatings from any artifact destruction during the sample preparation. The phase composition of YSZ coatings before and after thermal cyclic test was characterized by an x-ray diffraction (XRD, Bruker, D8 Advance, Germany) system. The porosity of the different regions of top-coat was determined by image analysis. The cross-sectional Vickers hardness was determined by a micro-Vickers Indenter (BUEHLER MICROMET5104 , Akashi Corporation , Japan). The hardness tests were performed at a test load of 300 g and holding time of 30 s. The in-plane Young's modulus of top-coat was measured by a Knoop indentation method. The parameters and the test system were the same with the measurement of microhardness.

2.3. Thermal cyclic test

To simulate the actual service condition and embody the thermal gradient across the TBCs, a gas burner test setup was designed for the thermal gradient cyclic test (Xi'an Jiaotong University, China). The preset temperature of 1150/940 °C were used to carry out the tests (1150 °C at top coating surface and 940 °C at backside surface, the bond coat temperatures were about 1000 °C.). Mass flowmeters with accuracy 0.1 SLM were employed to ensure the stability of the flame. The temperature gradient was controlled by adjusting the flow ratio of propane and oxygen. The temperatures of the specimen at surface and backside were monitored by non-contact infrared thermometers with wavelengths of 8–14 μm and 1.6 μm, respectively. The emissivity for YSZ and superalloy substrate was calibrated to be 1 and 0.91 according to their wavelength, respectively. The lifetime of TBCs was defined as the thermal cyclic lifecycles when 10% area delamination of the top coat was observed. One thermal cycle was defined as follow: heating process, the sample surface were heated to the range of preset temperature of 1150 ± 30 °C (about 70 s); the holding process, the temperature of sample surface sustain at 1150 ± 30 °C (about 50 s); the cooling process, the temperature of sample surface drop from 1150 ± 30 °C to about room temperature (about 120 s).

3. Results and discussion

3.1. The design principle of TBCs

Thermal insulation performance is one of the fundamental functions for thermal barrier coatings. In our previous study, "thermal resistance" is introduced to evaluate the thermal insulation effect of the thermal insulation performance of TBCs, and it is expressed as [25]:

$$R = \frac{\delta}{\lambda A} \tag{1}$$

where δ is the thickness of top coat, λ is the thermal conductivity and A is the area normal to the heat flow. For the specific TBCs, "thermal barrier performance" is a parameter independent on the area A, hence we introduce the unit thermal resistance (UTR) as an intrinsic parameter to describe the thermal insulation performance of TBCs, it can be expressed as

$$\mathrm{UTR} = \frac{\delta}{\lambda} \tag{2}$$

The thermal conductivity of DVC and lamellar structured YSZ top coat is taken as 1.75 $Wm^{-1}K^{-1}$ [19] and 1 $Wm^{-1}K^{-1}$ [22]. Under the principle of same unit thermal resistance, the thermal insulation effect of 1000 μm DVC YSZ is equal to 570 μm lamellar structured YSZ. In

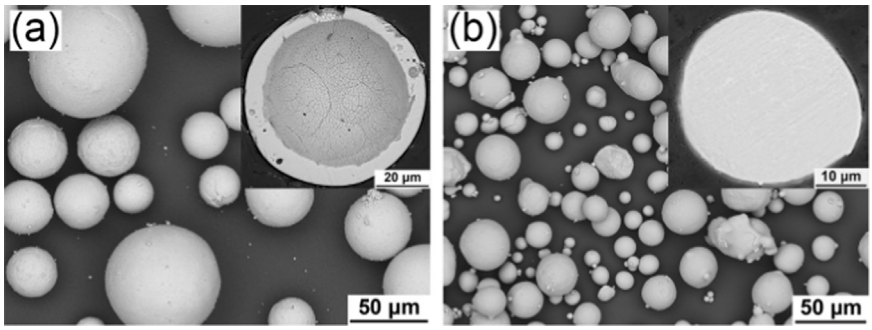

Fig. 1. Morphology of the spherical spraying powders used for top coat (a) and bond coat. The inset shows the cross section of an individual powder.

Table 2
Parameters of low-pressure plasma spraying for bond coat.

Parameters	Value
Arc current, A	575
Arc voltage, V	150
Plasma gas (Ar) flow, L/min	40
Plasma gas (H_2) flow, L/min	6
Powder feeding gas (Ar) flow, L/min	1
Chamber pressure, kPa	15
Spray distance, mm	280

this study, TBCs with same unit thermal resistance and thickness were prepared to comprehensively understanding the failure behavior of DVC and lamellar structured TBCs and provide further coating structure optimization solutions.

Fig. 2 shows three different groups of as sprayed TBCs, namely, 1000 μm lamellar YSZ TBCs (Fig. 2(a)), 1000 μm DVC YSZ TBCs (Fig. 2(b)), and 570 μm lamellar YSZ TBCs (Fig. 2(c)). In order to identify the three different groups of TBCs briefly, we name them with L1000, D1000, and L570. The TBCs were compared under the condition of same top coat thickness and unit thermal resistance. It is seen from the high magnified images of Figs. 2(d) and 2(c) that, the top coat shows a typical lamellar microstructure. The microstructure of DVC top coat is much denser. We examined the elastic modulus and porosity of the lamellar structure and DVC structure, shows in Table 3. It is seen that the value of elastic modulus and porosity of the two groups of TBCs are fairly close, (E: 63.9 ± 6.1 GPa and 64.1 ± 4.8 GPa for L1000 and L570, P: 12.1 ± 1.4% and 11.8 ± 0.6% for L1000 and L570). The DVC structure shows a higher elastic modulus (82.4 ± 7.1 GPa) and lower porosity value (7.1 ± 0.9%).

3.2. Thermal cyclic behaviors

Fig. 3 shows the lifetimes of different groups of TBCs after gradient cyclic test. Three samples were tested for each group, and the lifetime is the mean value. It is found from Fig. 3 that, the lifetime of dense vertically cracked TBC is about 2040 cycles, which is much longer than that of lamellar structured ones with same top coat thickness, proving that the DVC TBC is an effective way to prolong the TBC lifetime under this condition. It is identical with the results of the literature relevant to lifetime of DVC and lamellar TBCs [19,21,26]. However, the vertically cracks and dense structure weakened the thermal insulation performance, and it is reported that the thermal conductivity of DVC YSZ is about 75~80% higher than that of standard lamellar YSZ [19,21]. As mentioned above, we used the unit thermal resistance (UTR) to evaluate the thermal insulation performance of TBCs. L570 has the same UTR with D1000, but L570 shows no obvious sign to damage

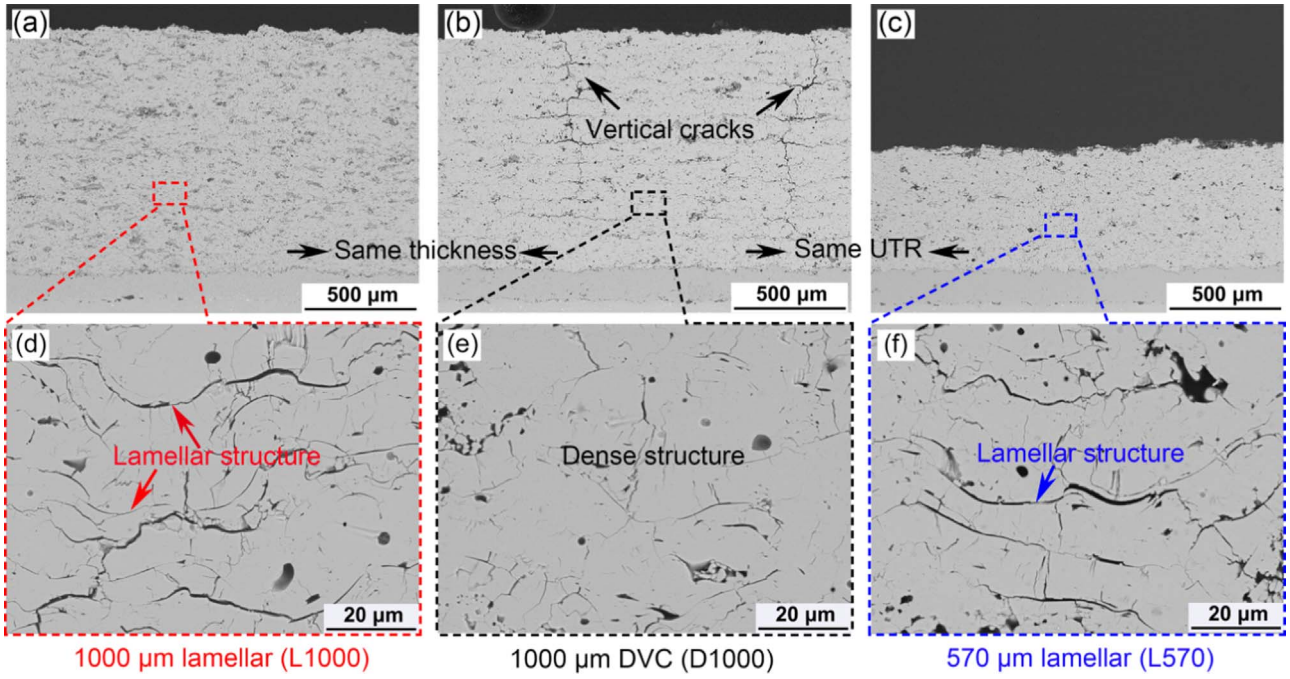

Fig. 2. Microstructure of TBCs with same top coat thickness (L1000 and D1000) or UTR(L570 and D1000). (a) 1000 μm lamellar (L1000), (b) 1000 μm DVC(D1000), (c) 570 μm lamellar (L570).

Table 3
Elastic modulus (in-plane) and porosity of the as sprayed TBCs.

Samples	E (GPa)	Porosity (%)
Lamellar 1000 μm	63.9 ± 6.1	12.1 ± 1.4
DVC 1000 μm	82.4 ± 7.1	7.1 ± 0.9
Lamellar 570 μm	64.1 ± 4.8	11.8 ± 0.6

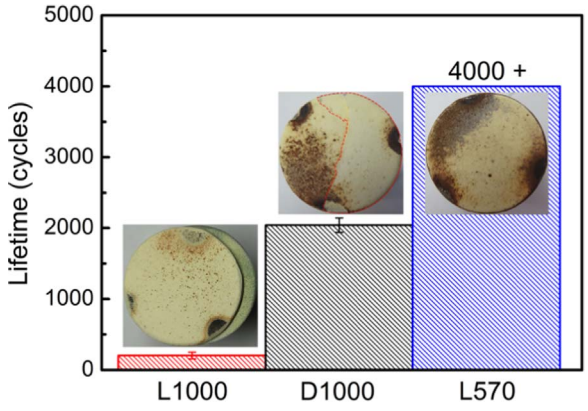

Fig. 3. Lifetimes of the TBCs after different cyclic test.

or spall off even the thermal cyclic test proceeded more than 4000 cycles. Under the condition of same UTR, the lifetime of L570 is at least two times higher of that DVC TBCs.

3.3. Failure mode

In order to clarify the failure mode of the three groups of TBCs, the cross sectional SEM images after different cyclic tests were examined. As is shown in Fig. 4, the low and high magnified images are shown to examine the specific failure mode. It is shown in Fig. 4(a) that, after about 203 cyclic tests, the whole top coat of L1000 spalled off, and the failure happened at the bond coat/top coat interface (shows in Fig. 4(d)). For the D1000 TBCs, it is seen from Fig. 4(b) that, although the failure happened near bond coat/top coat interface, there still remain a thin layer of 60–80 μm YSZ attached on the bond coat (shows in Fig. 4(e)). It may attribute to the dense structure increased the bond strength to the bond coat. For the L570 TBCs (shows in Fig. 4(c)), after more than 4000 cycles thermal cyclic test, the TBCs shows no obvious damage and the lifetime has reached nearly double of the D1000 TBCs.

3.4. TGO thickness

It has been reported that TGO growth is one of the dominant factors leading to the failure of TBCs [27,28]. During long time high temperature exposure, TGO growth is inevitable. But if the TGO thickness is not beyond the critical value of 5–6 μm, TGO thickening is not considered to be a dominant factor responsible for the failure of TBCs [29,30]. In this study, the as prepared samples with bond-coat were subjected to a two steps preheat-treatment to forming a dense and connective Al_2O_3 TGO. This will sharply decrease the growth rate of TGO [31]. We examined the TGO thickness of different group of TBCs after different cyclic tests, as is shown in Fig. 5. It is seen from Fig. 5(a) and (b) that, the TGO thickness are only 0.41 ± 0.04 μm and 0.96 ± 0.14 μm after thermal cyclic tests to failure, respectively. It is far below the critical value of 5–6 μm. For L570 TBCs, the TGO thickness is 1.1 ± 0.11 μm, shows in Fig. 5(c) and L570 survived more than 4000 cyclic tests. It is reasonable to believe that TGO thickening is not responsible for the failure of L1000 and D1000 TBCs.

3.5. Phase compositions of the top coat

For YSZ TBCs, phase transformation is considered to be another crucial factors leading to the failure of TBCs. The phase transformation from the as sprayed nontransformable t′ phase to tetragonal t phase and cubic phase (c-phase), and then from t phase to monoclinic phase (m phase) during long-term thermal exposure and cooling. The phase transformation from tetragonal t phase to monoclinic m phase accompanies 3–5% volume expansion, which may cause the failure of TBCs [32,33]. Fig. 6 shows the phase compositions of YSZ top coat for the as sprayed and after different thermal cyclic tests state. It is seen from Fig. 6 that, no obvious phase transformation are found for the L1000 and D1000 TBCs. Very little monoclinic phase peaks are found, but these peaks are even found in the as sprayed state. It is reasonable to believe that the high temperature exposure in this study did not cause the phase transformation of YSZ coatings, and phase transformation is not responsible for the failure of TBCs (Fig. 7).

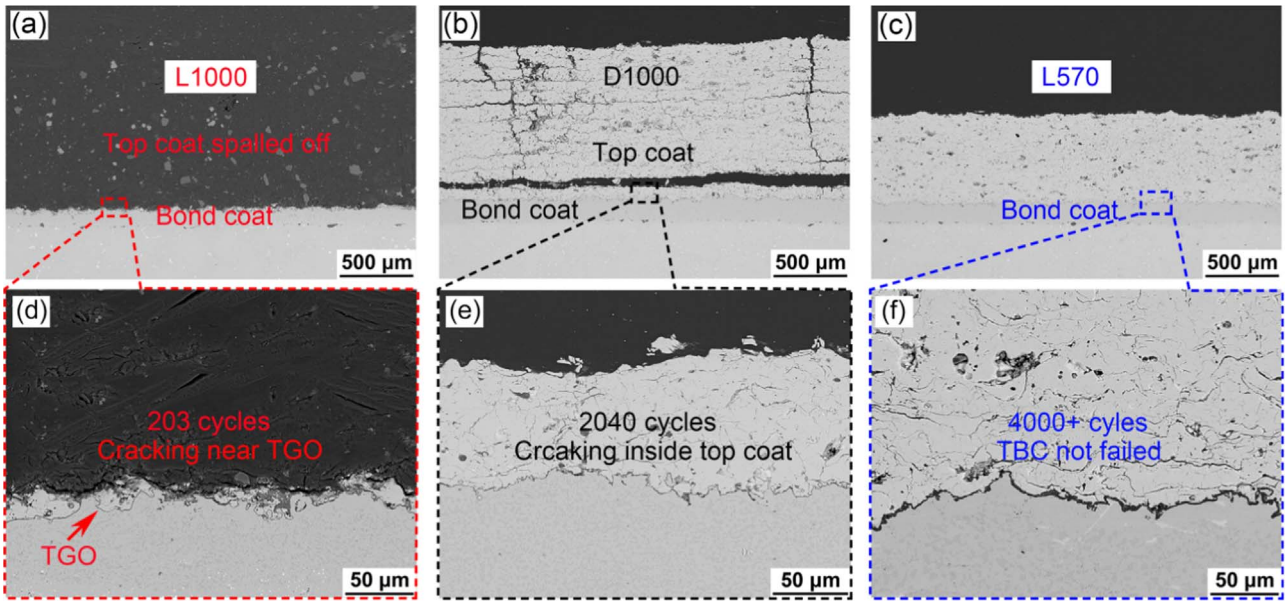

Fig. 4. Cross sectional images of different groups of TBCs after different cyclic tests.

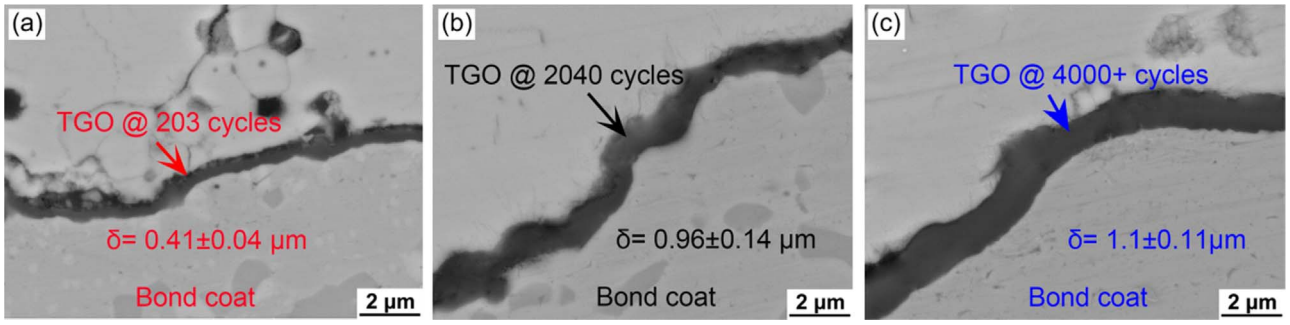

Fig. 5. Cross sectional images of near thermal grown oxide after different thermal cyclic test. (a) L1000, (b) D1000, (c) L570.

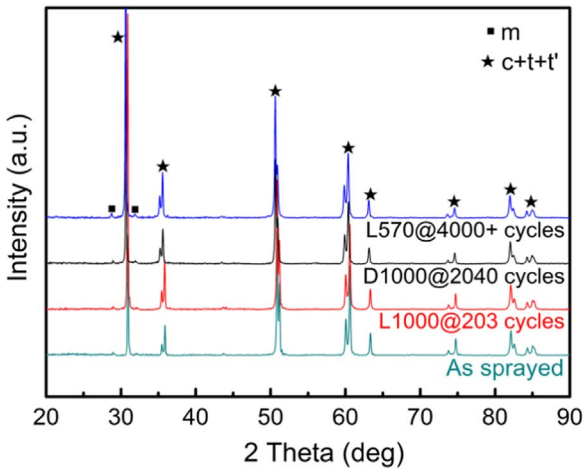

Fig. 6. XRD patterns of the YSZ top coat before and after thermal cyclic tests.

3.6. Mechanical evolution caused by the sintering of top coat

Under the real service conditions, TBCs are exposed to high temperature, which inevitably leading to the sintering of the ceramic top coat. Elastic modulus and hardness are often introduce to evaluate the degree of sintering [34–36]. The in-plane direction elastic modulus were employed to evaluate the sintering degree of different group of TBCs. Since the vertical cracks is a kind of special edge, the indentation on vertical cracks is lack of accuracy. Therefore, for D1000 coatings, only the elastic change on comparatively integrate part were indentated. Fig. 8 shows the elastic modulus and hardness of different groups of TBCs before and after thermal cyclic tests. It is seen from Fig. 8(a) that, the elastic modulus of the as sprayed lamellar structured L1000 and L570 are 63.9 ± 6.1 GPa and 64.1 ± 4.8 GPa, respectively. And for the DVC structured YSZ top coat, the elastic modulus of the as sprayed state is 82.4 ± 7.1 GPa, which is higher than that of lamellar YSZ. The higher modulus is related to the dense structure resulting from the top coat preparing process. With the proceeding of thermal cyclic tests, the elastic modulus of L1000 increased to 81.3 ± 10.6 GPa when the top coat spalled off the substrates, however, that of D1000 increased to 107 ± 10.0 GPa when the TBCs failure happens. It can be speculated that, the as sprayed D1000 presents a relatively high level of modulus result in a higher sintering start point. And on the other hand, the vertically cracks alleviated the strain caused by sintering process, which enable the top coat survived a longer high temperature exposure and may shrink freely to some degree. This eventually led to the high modulus of D1000 top coat. As for the L570, the elastic modulus of the top coat increased to 94.2 ± 9.8 GPa when the thermal cyclic tests proceeded more than 4000 cycles. However, the L570 shows no obvious failure and it has been confirmed from the high magnified images near TGO in Fig. 4(f). We believed that, the relative thinner top coat reduced the stress level of the TBC system, and eventually extend the thermal cyclic lifetime. As a result, we presented the modulus of L570 with narrow columns showing the low level TBC system stress. Fig. 8(b) shows the hardness of different groups of TBCs before and after thermal cyclic tests, it presents nearly a same trend with elastic modulus. It is believed that, the sintering of top coat mainly responsible for the failure of 1000 DVC and lamellar TBCs.

3.7. Analysis of thermal cyclic behavior

After investigating the thermal cyclic behavior of different structured TBCs, at least three aspects can be clearly distinguished. For the failed L1000 and D1000 TBCs, the thickest TGO thickness is 0.96 ± 0.14 μm, far below the critical thickness causing the top coat delamination. YSZ top coat shows no distinct phase transformation. The elastic modulus and hardness increased to different degrees after different thermal cyclic tests.

In this study, during the high temperature exposure process, the mechanic evolution dominate the failure behavior of the TBCs, specifically, the competition between the cracking driving force and

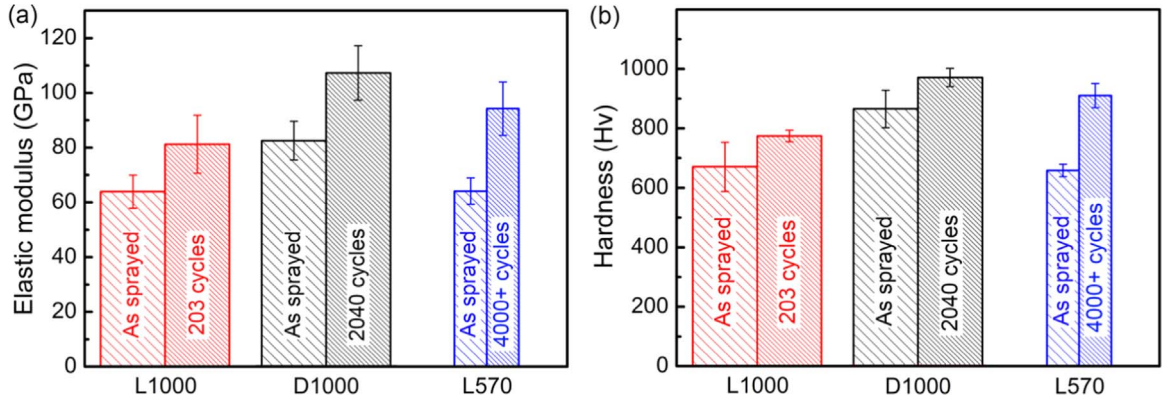

Fig. 7. Elastic modulus (a) and Vickers hardness (b) of the top-coat before and after thermal cyclic tests.

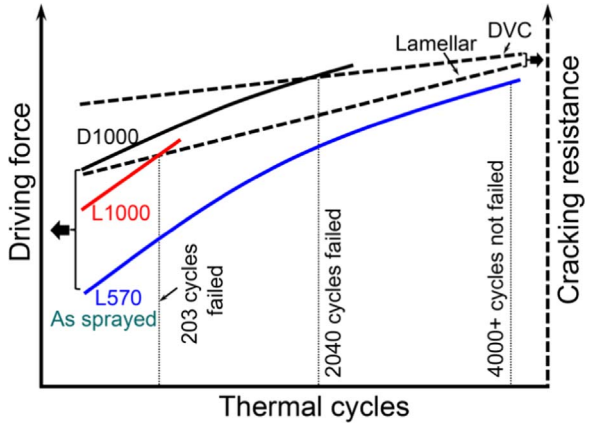

Fig. 8. Mechanical properties evolution of different groups of TBCs with the proceeding of thermal cycles.

the cracking resistance dominates the failure behavior. In order to analysis the failure behavior of the different group of TBCs, the strain energy release rate, G_h, is introduced to describe the driving force qualitatively, shows as follow:

$$G_h = \int_0^h \frac{E\ \varepsilon^2}{2(1-\nu)} dx \tag{3}$$

where h is the top coat thickness, E is the elastic modulus, ε is the strain, ν is the Poisson's ratio.

In this study, the relative thin layer of ceramic top coat is just from 570 to 1000 μm. However, the substrate is often several millimeters, for example 3.150 mm (738 alloy plus the bond coat) in this study. It is about 3–5 times thicker than top coat. What's more, the elastic modulus of YSZ is about less than 100 GPa due to porous structure, but the elastic modulus of superalloy is about 200 GPa, which is much higher than that of top coat. Therefore, it is the substrate dominates the strain of the TBC system. For the as-sprayed TBCs, there is a residual tensile stress in the top coat, and during thermal cycle test, the tensile stress increases. Therefore, the strain in top coat surface is always positive, and the negative strain should appear in the inner substrate. In a word, the strain in the top coat is always positive. Combining the expression of strain energy release rate in Eq. (1), it can be conclude that G_h increase with the coating thickness. We describe the mechanic evolution process of different groups of TBCs in Fig. 8. TBCs failed when the driving force is beyond the cracking resistance. It is seen from Fig. 8 that, the start point of the different groups of TBCs lies at different levels. D1000 shows the highest driving force level because of the relative thicker top coat thickness. Besides, the high level elastic modulus resulting from the preparing process increases the G_h to some degree, which leads to D1000 showing the highest driving force at the as sprayed state. For L1000, except for the thick top coat, the lamellar structure presents a porous feature and shows a lower modulus value. This is the reason for L1000 shows a lower driving force. L570 has the thinnest thickness and lamellar structure, which sharply decreased the driving force at the as sprayed state.

As we mentioned above, high temperature exposure inevitably caused the sintering of YSZ, and result in both the increase of driving force and cracking resistance. We showed the competition relationship of them during thermal cyclic test in Fig. 8 L1000 TBCs failed at 203 cycles, the thick top coat bring the TBC system high level of driving force and accumulated at the top coat/bond coat interface, and the driving force increased rapidly at the very beginning according to the our report on the two-stage sintering mechanism for TBC [37,38]. On the other hand, the cracking resistance of lamellar structured top coat stay at a low level and increased slower than the driving force. Therefore, when the driving force catches up or beyond the cracking resistance, L1000 failed. The lifetime of D1000 is rather higher than that of L1000, it is consistent with the report [18,19]. The dense top coat makes the driving force and the cracking resistance of D1000 higher than that of L1000. However, both of them increases slower because the sintering process has reached to the sintering stage II, a lower increasing rate. What's more, with the alleviation of vertically cracks, the rising of driving force was hindered. We believe the competition between driving force and cracking resistance sustains for a longer time and result in the extent of D1000 lifetime compared to L1000. What's more, we believe the vertically cracks accelerate the failure process at the later period of failure when they connected with the transverse cracks. At last, for L570 TBCs, the start driving force stays at a very low level because of the thinnest top coat thickness. With the proceeding of thermal cyclic test, both of driving force and cracking resistance increased. It takes a long time for the driving force catching up with the cracking resistance. L570 not failed after more than 4000 cyclic test.

4. Conclusions

In this study, three groups of YSZ TBCs with same top coat thickness and equivalent thermal insulation performance were designed and prepared, and they were also subjected to thermal gradient tests, with the aim to comprehensively understanding of the failure behavior of DVC and lamellar structured TBCs.

The following conclusions could be obtained from this work:

(1) Equivalent thermal insulation conception is introduced for the design of thermal barrier coatings. Lamellar structured TBCs showed more than double lifetime of DVC TBCs under equivalent thermal insulation condition, although the DVC TBCs extend the lifetime of lamellar TBCs with same top coat thickness.
(2) L1000 TBCs failed at top coat/bond coat interface due to the large driving force at the as sprayed state, and D1000 failed inner top coat because of the alleviate of vertically cracks and dense structure. L570 shows no obvious failure after more than 4000 thermal cyclic tests.
(3) The maximum thickness of TGO in the failed TBC samples is 0.96 μm, being far less than the critical value causing the failure of TBCs through complete delamination of the top coat. In addition, there was no obvious phase transformation during thermal cyclic test. Therefore, the TGO thickening and phase transformation were not the essential reasons responsible for the failure of TBC in the present study.
(4) The competition between driving force and cracking resistance dominate the lifetime and failure behavior of different structured TBCs. New design criteria should be founded based on the thermal insulation performance.

Acknowledgments

The present project is supported by National Basic Research Program (Grant No.: 2013CB035701), the National Science Foundation of China (Grant No.: 51671159), the Fundamental Research Funds for the Central Universities, and the National Program for Support of Top-notch Young Professionals.

References

[1] N.P. Padture, M. Gell, E.H. Jordan, Thermal barrier coatings for gas-turbine engine applications, Science 296 (2002) 280–284.
[2] W. Fan, Y. Bai, Review of suspension and solution precursor plasma sprayed thermal barrier coatings, Ceram. Int. 42 (2016) 14299–14312.
[3] R. Vaßen, M.O. Jarligo, T. Steinke, D.E. Mack, D. Stöver, Overview on advanced thermal barrier coatings, Surf. Coat. Technol. 205 (2010) 938–942.
[4] D.R. Clarke, M. Oechsner, N.P. Padture, Thermal-barrier coatings for more efficient gas-turbine engines, MRS Bull. 37 (2012) 891–898.
[5] B.Y. Zhang, G.H. Meng, G.J. Yang, C.X. Li, C.J. Li, Dependence of scale thickness on the breaking behavior of the initial oxide on plasma spray bond coat surface

during vacuum pre-treatment, Appl. Surf. Sci. 397 (2016) 125–132.
[6] J.J. Tang, Y. Bai, J.C. Zhang, K. Liu, X.Y. Liu, P. Zhang, Y. Wang, L. Zhang, G.Y. Liang, Y. Gao, Microstructural design and oxidation resistance of CoNiCrAlY alloy coatings in thermal barrier coating system, J. Alloy. Compd. 688 (2016) 729–741.
[7] F. Zhou, Y. Wang, Z. Cui, L. Wang, J. Gou, Q. Zhang, C. Wang, Thermal cycling behavior of nanostructured 8YSZ,SZ/8YSZ and 8CSZ/8YSZ thermal barrier coatings fabricated by atmospheric plasma spraying, Ceram. Int. 43 (2017) 4102–4111.
[8] R. Ghasemi, H. Vakilifard, Plasma-sprayed nanostructured YSZ thermal barrier coatings: thermal insulation capability and adhesion strength, Ceram. Int. 43 (2017) 8556–8563.
[9] K.P. Jonnalagadda, R. Eriksson, K. Yuan, X.H. Li, X. Ji, Y. Yu, R.L. Peng, A study of damage evolution in high purity nano TBCs during thermal cycling: a fracture mechanics based modelling approach, J. Eur. Ceram. Soc. 37 (2017) 2889–2899.
[10] C. Cai, S. Chang, Y. Zhou, L. Yang, G. Zhou, Y. Wang, Microstructure characteristics of EB-PVD YSZ thermal barrier coatings corroded by molten volcanic ash, Surf. Coat. Technol. 286 (2016) 49–56.
[11] N.A. Fleck, A.C.F. Cocks, S. Lampenscherf, Thermal shock resistance of air plasma sprayed thermal barrier coatings, J. Eur. Ceram. Soc. 34 (2014) 2687–2694.
[12] N. Chen, X.M. Song, Z.W. Liu, C.C. Lin, Y. Zeng, L.P. Huang, X.B. Zheng, Quantitative analysis of the relationship between microstructures and thermal conductivity for YSZ coatings, J. Therm. Spray. Technol. 26 (2017) 745–754.
[13] J. Cho, J. Park, J. An, Low thermal conductivity of atomic layer deposition yttria-stabilized zirconia (YSZ) thin films for thermal insulation applications, J. Eur. Ceram. Soc. 37 (2017) 3131–3136.
[14] A. Cipitria, I.O. Golosnoy, T.W. Clyne, A sintering model for plasma-sprayed zirconia TBCs. Part I: free-standing coatings, Acta Mater. 57 (2009) 980–992.
[15] A.C.F. Cocks, N.A. Fleck, Constrained sintering of an air-plasma-sprayed thermal barrier coating, Acta Mater. 58 (2010) 4233–4244.
[16] T.A. Taylor, Thermal barrier coating for substrates and process for producing it, EP, US 5073433 A, 1991.
[17] X. Chen, T. Ohnuki, S. Kuroda, M. Gizynski, H. Araki, H. Murakami, M. Watanabe, Y. Sakka, Columnar and DVC-structured thermal barrier coatings deposited by suspension plasma spray: high-temperature stability and their corrosion resistance to the molten salt, Ceram. Int. 42 (2016) 16822–16832.
[18] P. Bengtsson, T. Ericsson, J. Wigren, Thermal shock testing of burner cans coated with a thick thermal barrier coating, J. Therm. Spray. Technol. 7 (1998) 340–348.
[19] H.B. Guo, R. Vaßen, D. Stöver, Thermophysical properties and thermal cycling behavior of plasma sprayed thick thermal barrier coatings, Surf. Coat. Technol. 192 (2005) 48–56.
[20] R. Vaßen, F. Traeger, D. Stöver, Correlation between spraying conditions and microcrack density and their influence on thermal cycling life of thermal barrier coatings, J. Therm. Spray Technol. 13 (2004) 396–404.
[21] M. Karger, R. Vaßen, D. Stöver, Atmospheric plasma sprayed thermal barrier coatings with high segmentation crack densities: spraying process, microstructure and thermal cycling behavior, Surf. Coat. Technol. 206 (2011) 16–23.
[22] W. Chi, S. Sampath, H. Wang, Ambient and high-temperature thermal conductivity of thermal sprayed coatings, J. Therm. Spray Technol. 15 (2006) 773–778.
[23] M. Madhwal, E.H. Jordan, M. Gell, Failure mechanisms of dense vertically-cracked thermal barrier coatings, Mater. Sci. Eng. A 384 (2004) 151–161.
[24] L. Xie, D. Chen, E.H. Jordan, A. Ozturk, F. Wu, X. Ma, B.M. Cetegen, M. Gell, Formation of vertical cracks in solution-precursor plasma-sprayed thermal barrier coatings, Surf. Coat. Technol. 201 (2006) 1058–1064.
[25] H. Xie, Y.C. Xie, G.J. Yang, C.X. Li, C.J. Li, Modeling Thermal conductivity of thermally sprayed coatings with intrasplat cracks, J. Therm. Spray Technol. 22 (2013) 1328–1336.
[26] Z. Lu, M.S. Kim, S.W. Myoung, J.H. Lee, Y.G. Jung, I.S. Kim, C.Y. Jo, Thermal stability and mechanical properties of thick thermal barrier coatings with vertical type cracks, T. Nonferr. Metal. Soc. 24 (2014) s29–s35.
[27] C.G. Levi, E. Sommer, S.G. Terry, A. Catanoiu, M. Rühle, Alumina grown during deposition of thermal barrier coatings on NiCrAlY, J. Am. Ceram. Soc. 86 (2010) 676–685.
[28] A.G. Evans, D.R. Mumm, J.W. Hutchinson, G.H. Meier, F.S. Pettit, Mechanisms controlling the durability of thermal barrier coatings, Prog. Mater. Sci. 46 (2001) 505–553.
[29] A. Rabiei, A.G. Evans, Failure mechanisms associated with the thermally grown oxide in plasma-sprayed thermal barrier coatings, Acta Mater. 48 (2000) 3963–3976.
[30] H. Dong, G.J. Yang, C.X. Li, X.T. Luo, C.J. Li, Effect of TGO thickness on thermal cyclic lifetime and failure mode of plasma-sprayed TBCs, J. Am. Ceram. Soc. 97 (2014) 1226–1232.
[31] B.Y. Zhang, J. Shi, G.J. Yang, C.X. Li, C.J. Li, Healing of the interface between splashed particles and underlying bulk coating and its influence on isothermal oxidation behavior of LPPS MCrAlY bond coat, J. Therm. Spray Technol. 24 (2015) 1–11.
[32] G.D. Girolamo, C. Blasi, L. Pagnotta, M. Schioppa, Phase evolution and thermo-physical properties of plasma sprayed thick zirconia coatings after annealing, Ceram. Int. 36 (2010) 2273–2280.
[33] I.V. Mazilin, L.K. Baldaev, D.V. Drobot, E.Y. Marchukov, N.G. Zaitsev, Phase composition and thermal conductivity of zirconia-based thermal barrier coatings, Inorg. Mater. 52 (2016) 802–810.
[34] L. Xie, M.R. Dorfman, A. Cipitria, S. Paul, I.O. Golosnoy, T.W. Clyne, Properties and performance of high-purity thermal barrier coatings, J. Therm. Spray Technol. 16 (2007) 804–808.
[35] M. Shinozaki, T.W. Clyne, A methodology, based on sintering-induced stiffening, for prediction of the spallation lifetime of plasma-sprayed coatings, Acta Mater. 61 (2013) 579–588.
[36] Y.Z. Liu, S.J. Zheng, Y.L. Zhu, H. Wei, X.L. Ma, Microstructural evolution at interfaces of thermal barrier coatings during isothermal oxidation, J. Eur. Ceram. Soc. 36 (2016) 1765–1774.
[37] G.R. Li, H. Xie, G.J. Yang, G. Liu, C.X. Li, C.J. Li, A comprehensive sintering mechanism for TBCs-Part I: an overall evolution with two-stage kinetics, J. Am. Ceram. Soc. 100 (2017) 2176–2189.
[38] G.R. Li, H. Xie, G.J. Yang, G. Liu, C.X. Li, C.J. Li, A comprehensive sintering mechanism for TBCs-Part II: multiscale multipoint interconnection enhanced initial kinetics, J. Am. Ceram. Soc. ⟨http://dx.doi.org/https://doi.org/10.1111/jace.14940⟩.